Carbon Mapper
Airborne System

Description of Technology

Version 1.0.0
Document Status: Approved
Document Owner: Daniel Bon, Daniel Cusworth, Riley Duren
Description: Description of Technology, submitted document

Date: October 1st, 2024

Carbon Mapper, Inc.
Pasadena, CA
https://carbonmapper.org/
data@carbonmapper.org

TABLE OF CONTENTS

1.0 Overview and Theory

Carbon Mapper commissions wide-area aerial surveys of oil and gas operations and other methane emitting regions with high precision imaging spectrometer instruments designed by NASA's Jet Propulsion Laboratory (JPL) that are calibrated and operated on various aircraft by JPL and other partners such as Arizona State University. These instruments, collectively referred to here as the Airborne Visible Infrared Imaging Spectrometer (AVIRIS) series, measure ground-reflected solar radiation with fields of view, spatial resolution, and detection limit that vary with aircraft altitude. These instruments measure radiance in the visible and shortwave infrared (VSWIR) region of the electromagnetic spectrum from 380–2510 nanometers (nm).

Carbon Mapper's airborne imaging spectrometer data processing and quality control pipeline is sensor agnostic and applies equally well to all sensors in this class. The "AVIRIS-series" covered by this ATM includes the Next Generation AVIRIS (AVIRIS-NG), AVIRIS-3, and AVIRIS-5 instruments operated by JPL, the VSWIR spectrometer on the Global Airborne Observatory (GAO) operated by Arizona State University, and the 3 NEON imaging spectrometer (NIS) instruments JPL built for the the National Science Foundation's National Ecological Observatory Network (NEON).

2.0 Instrument & Process Description

The hardware of AVIRIS-class of imaging spectrometers is well described in the peer reviewed literature (Asner, 2012, Hamlin 2011, and Mouroulis, 2018) and will only briefly be summarized here. Carbon Mapper contracts with aircraft operators including JPL and ASU for collection and preprocessing of calibrated radiance data cubes.

Carbon Mapper works with the instrument operators to develop and execute flight plans to meet data collection objectives for deployment campaigns, each typically lasting 2-4 weeks. Operators are responsible for instrument characterization and field calibration as well as flight operation and data acquisition. Imaging spectrometers are mounted in the aircraft in a downward looking orientation, and collect data in a pushbroom scanning mode (Figure 1).

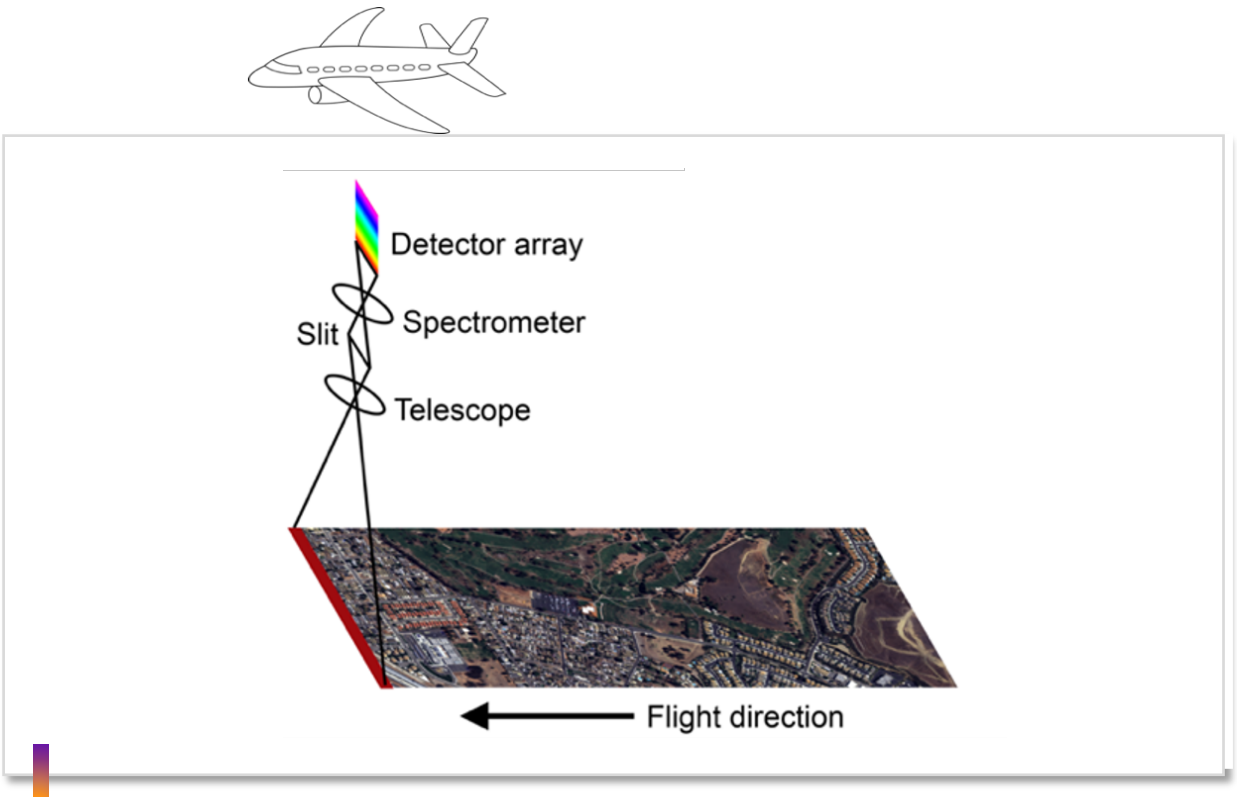

Figure 1. Diagram showing downward deployment of an AVIRIS-class instrument from an airborne platform.

2.1 Optical System

An AVIRIS-class imaging spectrometer instrument is a pushbroom linear array based on the Offner or Dyson optical configurations (Figure 2; Asner et al., 2012; Green et al., 2024). These instruments measure upwelling spectral radiance in 5 nm to 7 nm increments resulting in 350-450 contiguous spectral bands. These instruments were designed and tested to ensure greater than 95% cross-track spatial uniformity and spectral uniformity at all wavelengths. A simplified schematic of the Offner and Dyson optical systems is shown in Figure 2. In both cases, the "pushbroom" sensor images a line on the ground in the cross-track direction while the aircraft provides the along-track motion. A telescope projects the image of the line onto the spectrometer entrance slit. The spectrometer including a reflective grating that projects the spectrally dispersed light onto a low noise two dimensional Focal Plane Array (FPA), with spatial information in one axis and spectral information in the other. This allows the instrument to collect two dimensional images of the earth's surface where every pixel functions as a hyperspectral spectrometer. Offner VSWIR imaging spectrometer instruments (AVIRIS-NG, GAO, NEON) are still widely used, but the newer generation Dyson design (AVIRIS 3, AVIRIS 5, EMIT, Tanager) offer higher optical throughput, resulting in improved Signal to Noise Ratio (SNR) in a more compact and lightweight package.

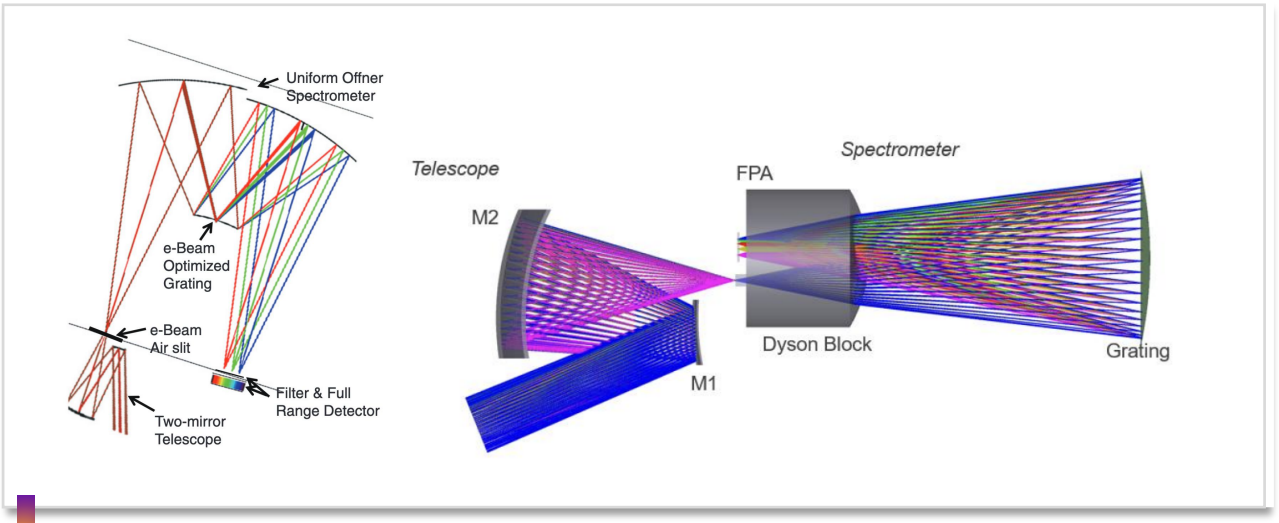

Figure 2. Schematic for the Offner (let panel) and Dyson (right panel) optical configurations (Asner et al., 2012; Green et al., 2024; respectively).

2.2 Collection and Calibration of Spectral Radiance

Details of the calibration process for AVIRIS-class imaging spectrometers can be found in Chapman, *et. al,* 2019. Figure 3 shows a schematic for the correction of electronic and optical effects and application of absolute calibration coefficients to generate calibrated radiance cubes.

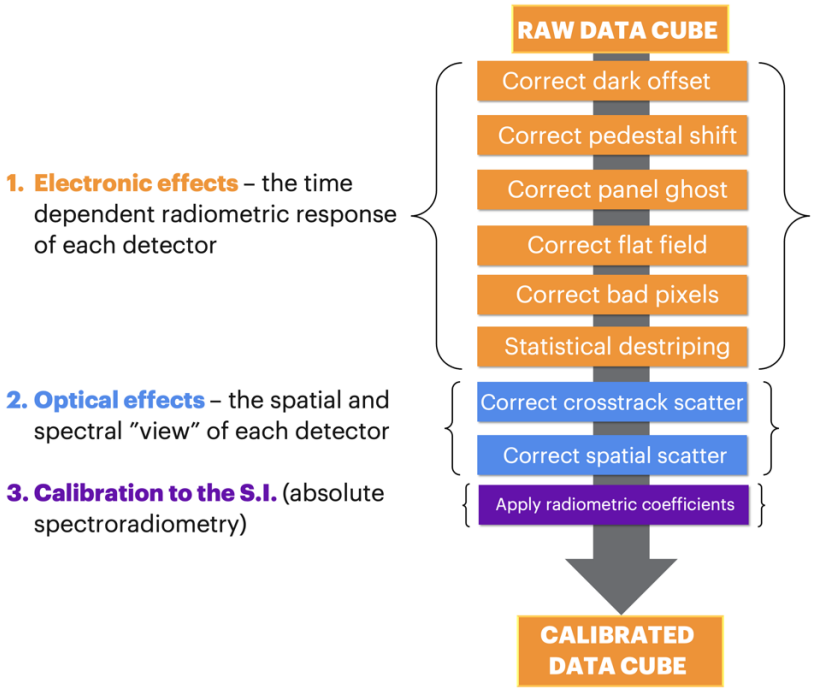

Figure 3. Processing of raw data to raw calibrated radiance is shown in this figure from Chapman, et al., 2019.

Radiometric coefficients are determined for each deployment through a process of using a NIST-calibrated standard irradiance lamp.

Carbon Mapper uses a data product model as shown in Figure 4. Raw observations are designated Level 0 (L0) and calibrated radiance data is designated Level 1 (L1). The Level 3 (L3) and Level 4 (L4) products shown here are the basis of information submitted to the EPA Super Emitter Program.

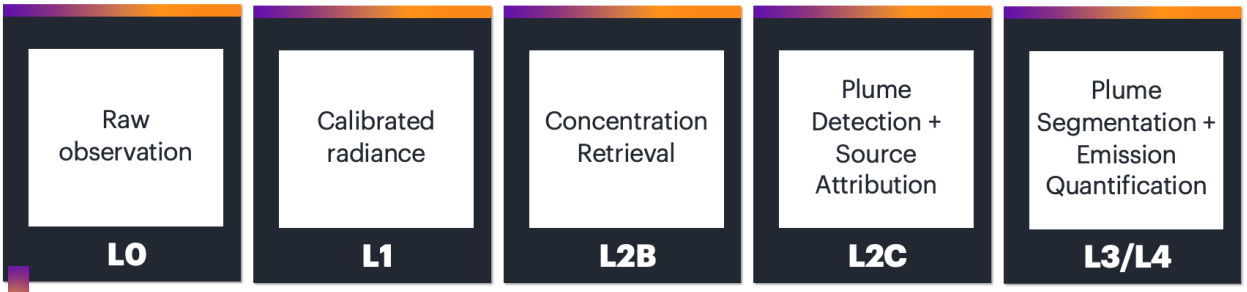

Figure 4. Simplified data flow indicating the Carbon Mapper data processing pipeline and product levels. More details are provided in the Carbon Mapper product guide and algorithm theoretical basis documents included in this application. The most current versions of these documents are available at https://carbonmapper.org/resources/technical-resources

2.3 Navigation Instrumentation and data Orthorectification

Each aircraft is also equipped with an Inertial Measurement Unit (IMU) co-located with the imaging spectrometer sensor that records the sensor attitude, position and velocity with update rates > 100 Hz to support post flight analysis including reconstruction of observing geometry and orthorectification of spectrometer images.

2.4 Operational Parameters and Data Collection

Instrument specifications for airborne deployment of Offner and Dyson imaging spectrometry instruments are summarized in Table 1.

Specification	Value
Spectral Range	380–2510 nm
Spectral Sampling	5-7 nm
Bands used for methane quantification	2100 - 2500 nm
Ground Sampling Distance	3-14 m*
Swath Length	Typically > 15 km
Swath width	Typically 2-9 km*
Field of View	34-40°
Signal-to-noise at 2300 nm	400-1500
Flight Speed	150-300 knots
Flight Altitude	Typically 3-14 km

Table 1. Specifications for typical airborne deployments of AVIRIS-class airborne imaging spectrometers. *indicates quantities that vary with altitude.

2.5 Orthorectification and Radiance Processing

Raw digital signal data (L0) is processed to calibrated radiance at the conclusion of a flight deployment day. This processing also combines aircraft IMU data to provide geolocation arrays that are used to orthorectify imagery. Calibrated radiance data is then shipped to Carbon Mapper directly or delivered to a data repository (e.g., Oakridge National Laboratory Distributed Active Archive Center (DAAC)), where additional algorithmic processing for methane retrieval (L2), plume detection and segmentation (L3), and emission quantification (L4) are performed. For some field campaigns, the flight crew runs Carbon Mapper concentration retrieval algorithms in the field and delivers that data directly to Carbon Mapper, where additional plume detection and quantification processes are then performed. Raw (L1) radiance data is archived to allow for future reprocessing of data using future versions of Carbon Mapper processing algorithms as needed.

2.6 Methane Retrieval

Carbon Mapper operationally implements a columnwise matched filter (CMF) to estimate pathlength enhancements of CH4 (units ppm-m) relative to the background. This retrieved quantity has an equivalent interpretation as dry air column average enhanced mole fraction (units ppm) or column density of enhanced methane (kg m^{-2}) as reported by other passive remote sensing data providers. Each retrieval takes as input L1B non-orthorectified radiance data and outputs column CH4 concentration enhancements. The benefits of a CMF algorithm include fast computation and normalization of nonuniformities across sensor elements across the focal plane array. The retrieval utilizes SWIR windows where CH4 exhibits strong absorption: 2100-2480 nm.

2.6.1 Columnwise Matched Filter

The CMF algorithm seeks an estimate for concentration length of methane or CO2 ($\hat{\alpha}$) in units in parts per million meter (ppm-m) for each observed spectrum (Thompson et al., 2016; Thompson et al., 2015). This is done by testing each observed spectrum against a target signature ($\vec{t}$), accounting for noise and background covariance $\mathbf{\Sigma}$. At sensor radiance $\overrightarrow{L_m}$ (unit μW cm^{-2} sr^{-1} nm^{-1}) for a pixel affected by enhanced gas concentration is modeled through Beer-Lambert's Law:

$$\overrightarrow{L_m} = \overrightarrow{L_0} e^{-\vec{k}\alpha} \quad (1)$$

Where $\overrightarrow{L_0}$ represents at-sensor radiance in presence of background levels of a gas, and $\vec{k}$ represents gas absorption. This model can be further simplified using Taylor expansion, assuming an optically thin plume:

$$\overrightarrow{L_m} \approx \overrightarrow{L_0} - \alpha\vec{t}(\overrightarrow{L_0}) \quad (2)$$

Where $\vec{t}(\overrightarrow{L_0}) = \vec{k} * \overrightarrow{L_0}$, the unit absorption spectrum, as is calculated through radiative transfer simulations of transmittance. To estimate $\overrightarrow{L_0}$, we use the mean spectrum $\vec{\mu}$ for all pixels in a "column" (i.e., all pixels in the flight direction of a single cross-track element; Figure 4) of observed data:

$$\overrightarrow{L_m} \approx \vec{\mu} - \alpha\vec{t}(\vec{\mu}) \quad (3)$$

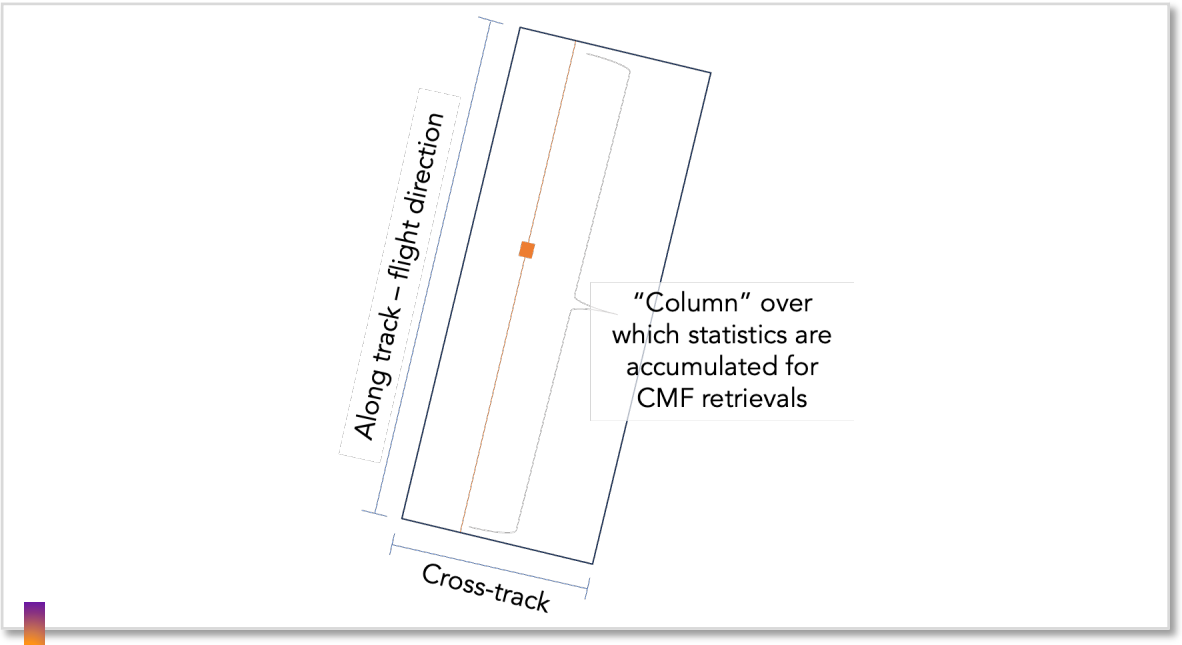

Figure 5. Simplified diagram of an image collection as it pertains to along and cross tracks - including which pixels are used in CMF algorithms.

The optimal value $\hat{\alpha}$ is found through optimization of log-likelihood - e.g., for the *i*th spectrum, $\hat{\alpha}_i$ is the solution that minimizes the residual between observed and modeled spectra while accounting for covariance. The maximum likelihood solution takes the following form (Foote et al., 2021):

$$\hat{\alpha} = \frac{\vec{t}^T \Sigma^{-1}(\overrightarrow{L_m} - \vec{\mu})}{\vec{t}^T \Sigma^{-1}\vec{t}} \quad (4)$$

2.6.2 Covariance Estimation

The covariance matrix **Σ** is estimated from these same pixels in the across-track column. We employ a low-rank approximation for covariance in order to stabilize the solution in Equation 4, especially under regimes of few pixels per column. This approach is explained in more detail in Thompson et al. (2015) and Manolakis et al. (2009), but briefly we decompose the covariance matrix into *p* eigenvalues (ϕ) and eigenvectors ($\vec{q}$):

$$\boldsymbol{\Sigma} = \sum_{i=1}^{p} \boldsymbol{\phi_i}\overrightarrow{\boldsymbol{q_i}}\overrightarrow{\boldsymbol{q_i}}^T \quad (5)$$

We approximate the inverse using the top 30 eigenvectors (*d*=30):

$$\Sigma^{-1} = \frac{\mathbf{1}}{\boldsymbol{\beta}}\left(\boldsymbol{I} - \sum_{i=1}^{d}\left[\frac{\boldsymbol{\phi_i} - \boldsymbol{\beta}}{\boldsymbol{\phi_i}}\right]\overrightarrow{\boldsymbol{q_i}}\overrightarrow{\boldsymbol{q_i}}^T\right) \quad (6)$$

Where

$$\beta = \frac{1}{p-d}\left(tr(\Sigma) - \sum_{i=1}^{d} \phi_i\right) \quad (7)$$

2.6.3 Unit Absorption Spectrum

The unit absorption spectrum is defined as the change in transmittance that relates to a perturbing signal $\vec{t}$. Recent work using airborne campaigns explored the sensitivity of CH4 matched filter retrievals to solar zenith angle (SZA), water vapor, and ground elevation (Foote et al., 2021). For example, larger SZAs mean longer path lengths from the sun to the sensor, resulting in deeper absorption per unit enhancement of CH4 (Figure 5).The impact on CH4 retrievals and flux estimates was smaller, with IME changing by ~ +/- 25%.

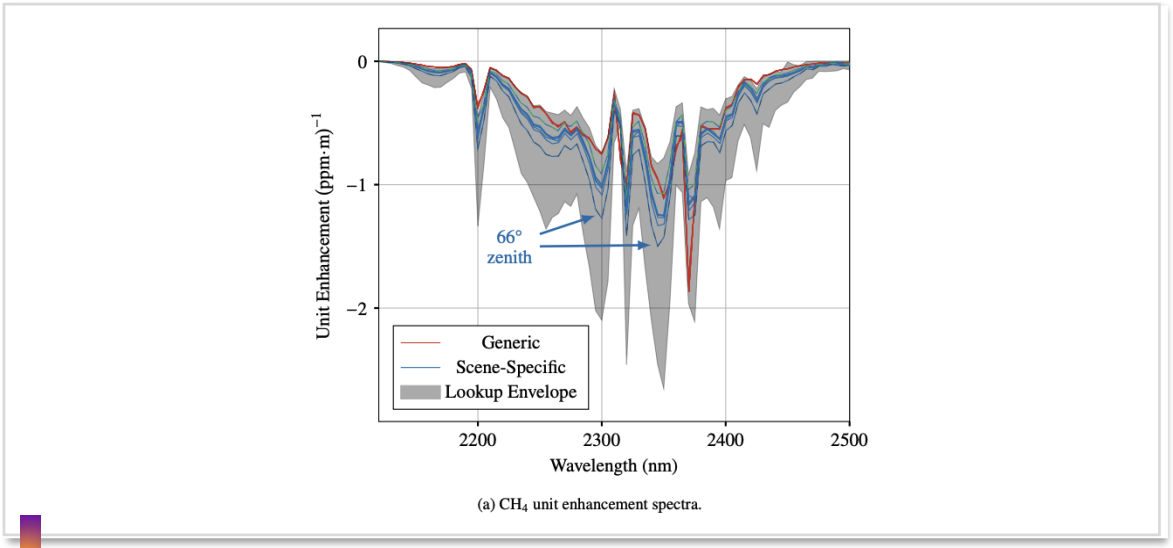

Figure 6. Dynamic unit absorption spectra ($\vec{t}$) for CH4. Blue lines represent unit absorption spectra for different solar zenith angles. Figure taken from Foote et al. (2021).

We follow the approach described in Foote et al., (2021) and select a scene-specific unit absorption for each observation for retrievals of CH4. For column water vapor content, for each image acquisition, we query either the High Resolution Rapid Refresh meteorological product in the U.S. or the ECMWF IFS meteorological product outside the U.S. For these dynamically queried or calculated parameters, we query a lookup-table database of unit absorption spectra that were precompiled and interpolated via MODTRAN simulations of various SZAs, water vapor concentration, CH4 background concentration, and surface heights (Foote et al., 2021).

More detail on Carbon Mapper's methane retrieval can be found in the L2b Algorithm Theoretical Basis Document (ATBD) attached to this submission. The most up-to date versions of all of Carbon Mapper's ATBDs can be found at https://carbonmapper.org/resources/technical-resources

2.7 Plume Identification and Marking

Carbon Mapper's analysts review match-filter retrievals to identify unique methane plumes that are connected and attributable to facilities, infrastructure, and potential individual operators. CH_4 emissions from unique point sources appear as higher atmospheric concentrations (enhancements) in the vicinity of the source. Enhancements undergo dispersion in the atmosphere that varies with a number of factors including emission rate, source elevation, wind speed and direction, terrain, and turbulence. Enhancements appear as a plume of gas extending from the emission source - similar to smoke from a fire. In other cases, for example in the presence of calm or no wind, the plume can appear as a blob centered over the source.

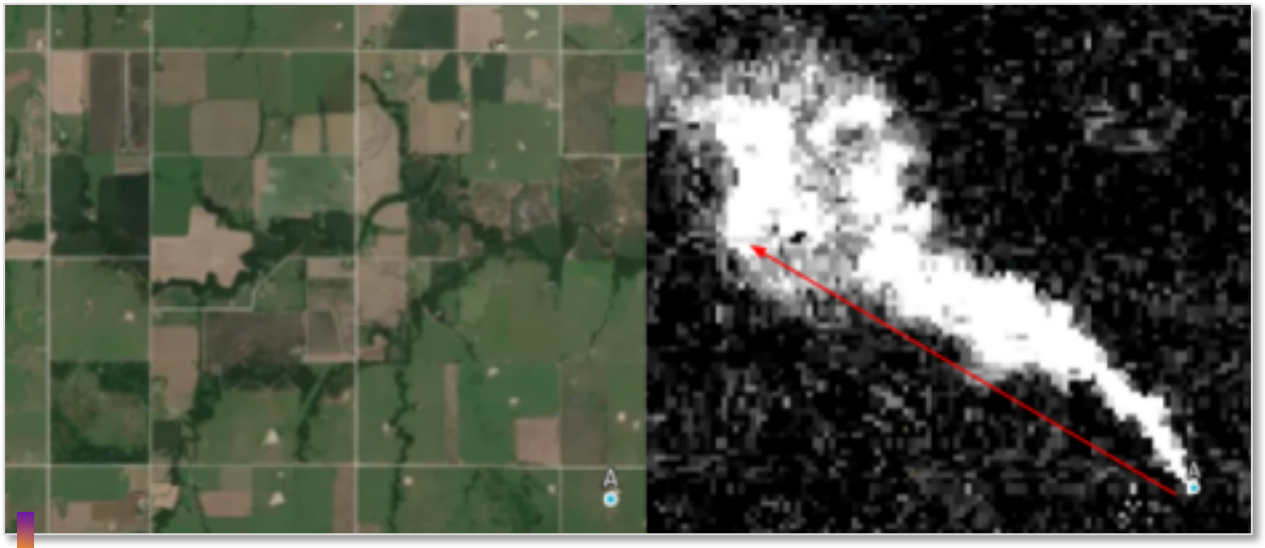

Figure 7. Left panel shows a true color (RGB: red-green-blue) image (provided by Google, Maxar Technologies) and the right panel shows the same scene in the matched filter retrieval. There is a clear plume in the matched filter retrieval. The red arrow indicated the wind direction.

Real (physical) plumes generally have the following characteristics:

- They do not strongly correlate with surface features like roofs, roads, or mineral outcroppings
- Exhibit more coherent signal than the background
- With sufficient wind, will become elongated in shape (like a smoke plume)
- Becomes increasingly diffuse at greater distances downwind of the source
- Appear to originate from surface infrastructure, recognizable in RGB overlay

The matched filter output in Figure 7 shows an example of a plume enhancement: it appears bright and exhibits a more coherent shape than the background pixels. The plume is most prominent towards its source in the lower right corner of the image and becomes more diffuse downwind toward the upper left corner. The RGB/satellite imagery on the left confirms that this is an oil and gas field and that the plume origin appears to be associated with a physical source on the ground (in this case a well pad).

Once a plume has been identified, visible imagery is used to discern apparent enhancements and distinguish between methane and eliminate enhancements that arise due to surface features or other artifacts (e.g. smoke, glint, glare from flares). Airborne scenes and match filters typically have pixel resolutions of about 3-14m. Carbon Mapper portal basemap images, provided by Mapbox, typically have resolution of less than 1 meter. Google, Maxar and Planet SkySAT basemaps with similar resolutions are also used for infrastructure identification as needed. Attributed plume origins therefore must overlap with an area of high concentration enhancement and plausibly-emitting surface infrastructure. Other atmospheric enhancements that do not satisfy this criteria (e.g., a downwind diffuse enhancement not connected to an emission source) are not attributed and would not be submitted to the super-emitter program.

The plume identification and processing step output is an origin location (latitude, longitude) for a plume given a unique concentration map (units in column enhancement CH4 (units ppm-m)). A more detailed description of plume marking processes can be found in Carbon Mapper's QC guide. The current version of this document has been submitted with this application and the most up-to-date version can be found at https://carbonmapper.org/resources/technical-resources

During blinded controlled release experiments conducted with average pixel sizes of about 5 meters, several Carbon Mapper analysts independently attributed each plume detection to latitude/longitude and found average agreement within 6 m radially from the known release point. In practice, this behavior is typical in the field. Figure 8 shows an example of a persistently emitting source detected across multiple flight days in the Permian Basin, TX. Carbon Mapper, following the protocols outlined above, with 5 meter pixels consistently marked the origin of each plume to within 6 meters of the only visible isolated infrastructure in close proximity. These results indicate that even at the maximum pixel size of 14 m for Carbon Mapper aircraft, the plume geolocation accuracy is predicted to be well below EPA's 50 meter requirement.

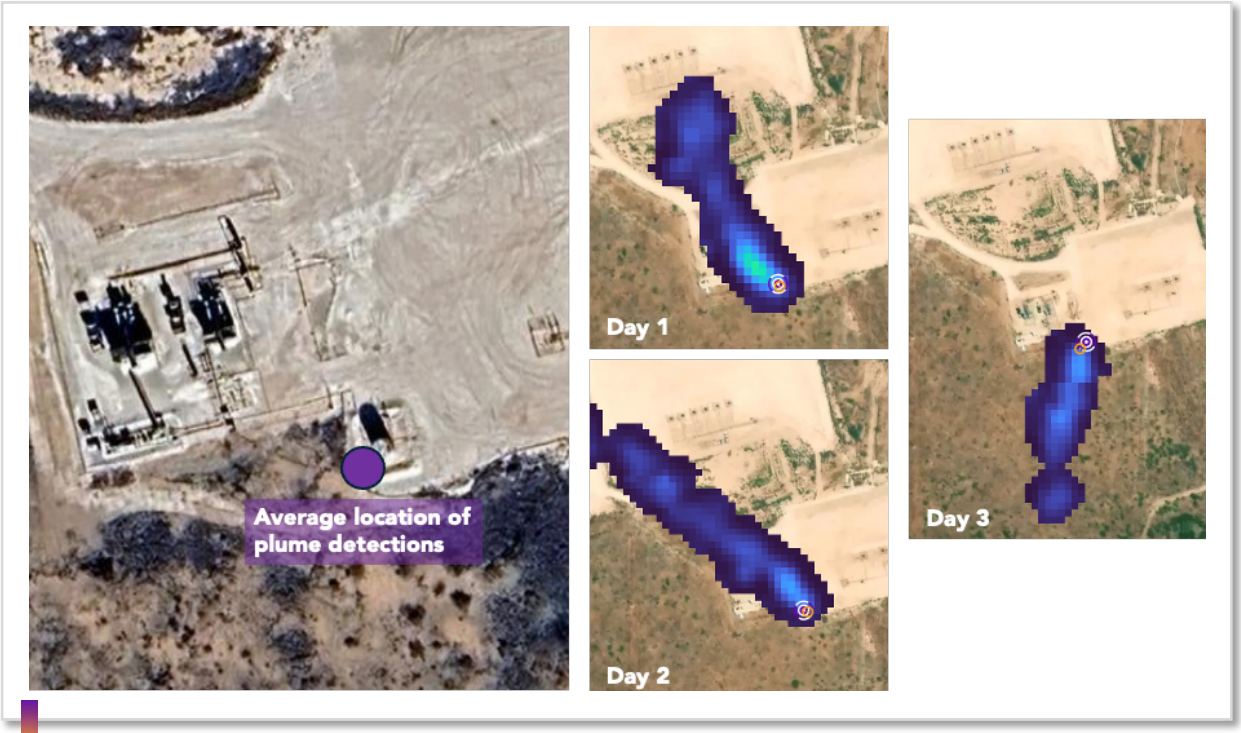

Figure 8. Example of multiple plume detections from Carbon Mapper aerial campaigns, observed across multiple flight days. Orange dots on each plume imagery describe where the analyst marked the origin of the emission source, using the protocols outlined in this document. The purple dots represent the average of all detections. Basemap provided by Google, Maxar Technologies.

2.8 Plume segmentation and emission quantification

Carbon Mapper implements an automated plume segmentation and delineation process on plumes identified and geolocated during the plume identification and marking process described above. The L3 process then segments a plume around this origin point to create a masked plume boundary that is used for mass and emission quantification. The segmentation algorithm proceeds as follows (visual example in Figure 9):

1. A concentration map is cropped around the origin of a plume: +/- 1000 meters in both directions
2. A concentration threshold is dynamically determined to separate lingering background enhancements from plume enhancements. This threshold is subtracted off the cropped concentration map around the plume origin.
3. Connected pixels of enhanced concentration (> ppm-m threshold) are grouped together. A cluster must contain 10 pixels to be considered part of the plume.
4. Clusters are then grouped if they fall within 2 pixels of each other.
5. Finally, a proximity metric is enforced on each cluster group. Separated clusters that exceed 15 pixels from the plume origin are excluded from the plume

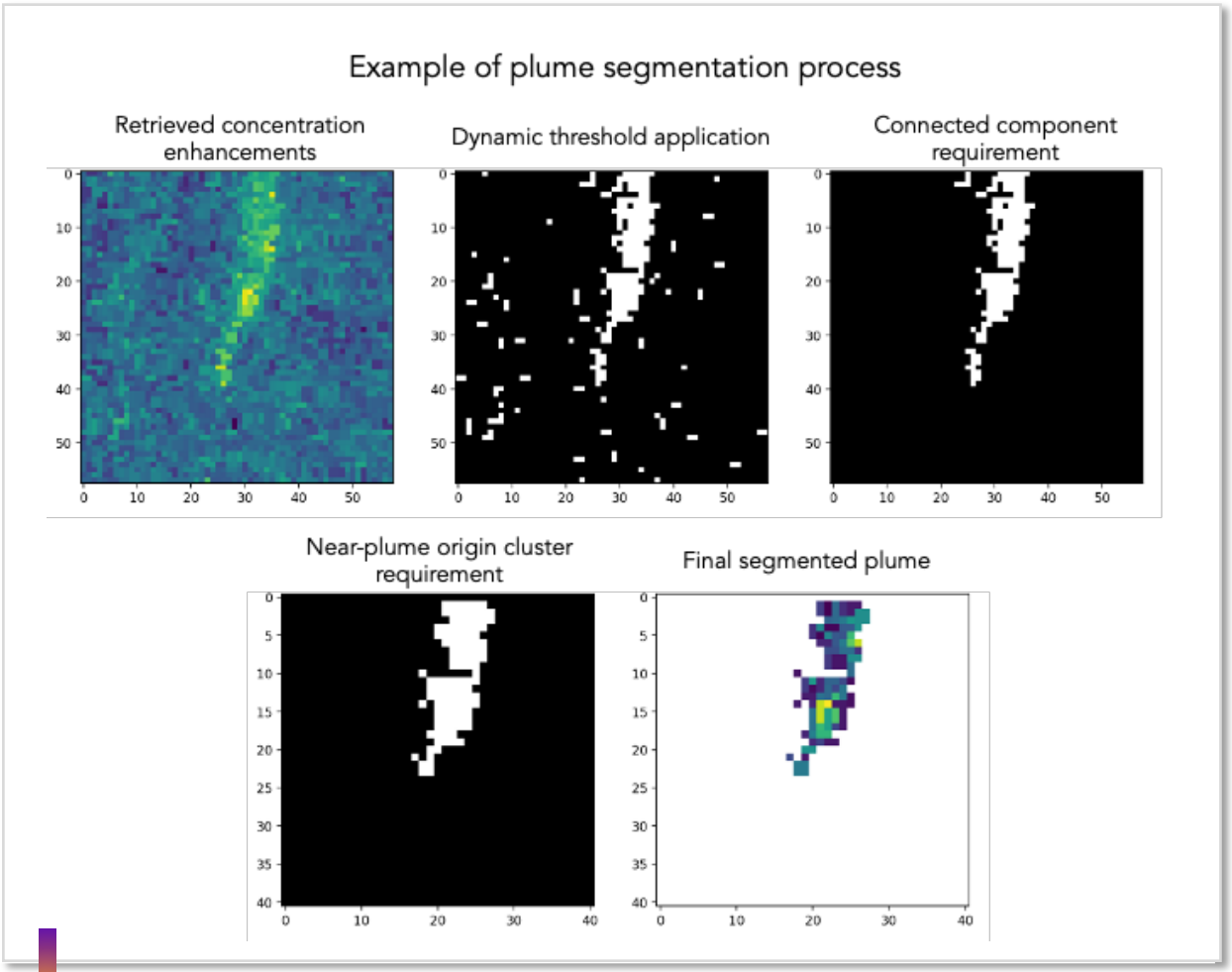

Figure 9. Visual example of plume segmentation processed applied to a detected CH4 plume.

Step 2 - determining a concentration threshold - has the largest impact on plume segmentation. For each plume, we seek a dynamically estimated threshold, based on the noise/background concentration information in the immediate vicinity around a plume. Thresholds are parameterized as a percentile of all pixels within a cropped distance around the origin of the plume (example shown in Figure 10a). Selection of a proper percentile/crop threshold is estimated by comparing to independent releases (e.g., controlled releases). Figure 10b demonstrates how concentration threshold varies as a function of crop lengths and percentile applied to retrieved concentrations. There is a consistent, strong relationship between crop and percentile: concentration thresholds stay roughly fixed against a set of crop/percentile parameters as shown in Figure 10. Therefore we seek a segmentation solution across a set of crop/percentile pairs that result in consistent concentration thresholds.

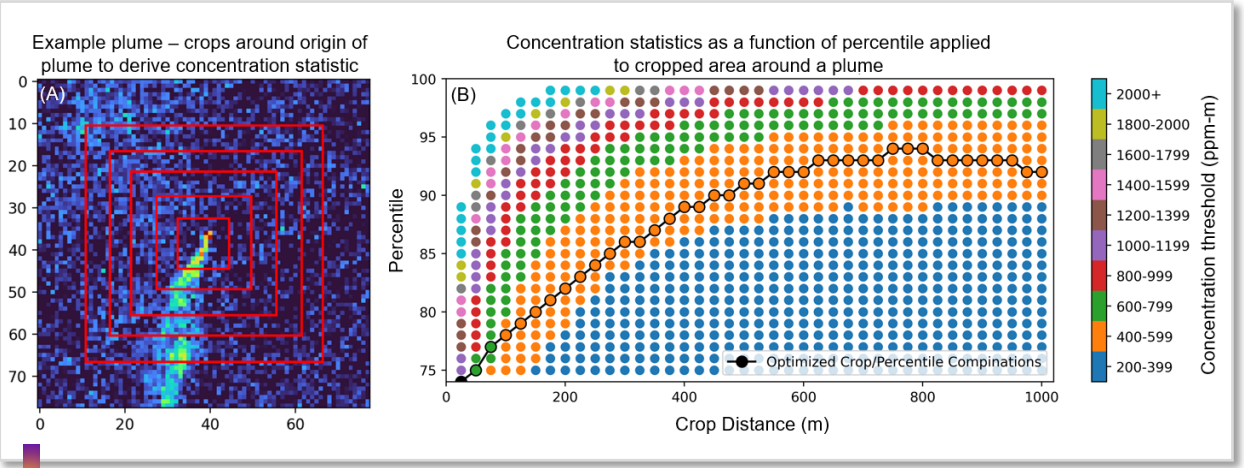

Figure 10. The process of cropping an image of retrieved concentrations around the origin of a plume (panel A). Concentration thresholds (units ppm-m) as a function of spatial crop around a plume and percentile of retrieved

concentrations within that crop for a set of controlled release plumes (panel B). The black line represents the optimized set of crop/percentile pairs we apply to detected plumes.

To find the best set of crop/percentile pairs, we perform an optimization procedure where emission rates are calculated for a benchmark of controlled release plumes under a variety of crop/percentile threshold candidates. To compare against independent data, segmented plumes must be processed to emission rate estimates. This is done by incorporating the Integrated Mass Enhancement (IME; units kg; Thompson et al., 2016) approach, which calculates the excess mass emitted to the atmosphere from a source:

$$IME = \alpha \sum_{i=1} \Omega_i A_i \quad (8)$$

Where *i* refers to a single plume pixel, Ω is the concentration enhancement of that pixel, α is a unit conversion scalar (from ppm-m to kg m^{-2}), and *A* is the area of that pixel (m^2). We calculate an emission rate Q using the following relationship (Ayasse et al., 2023):

$$Q = \frac{IME}{L} U \quad (9)$$

Where U is the 10-m wind speed (m s^{-1}) and *L* is the plume length (m). Here U is taken from the High Resolution Rapid Refresh (HRRR) 3km, 60 minute reanalysis product in the U.S. and the ECMWF IFS 9 km outside the U.S. Comparisons (Figure 11) of these gridded forecast products to 10 m weather station data in the U.S. (via the Synoptic Weather Data API: synopticdata.com) show high scatter for any data point, and roughly 1 m/s mean absolute bias.

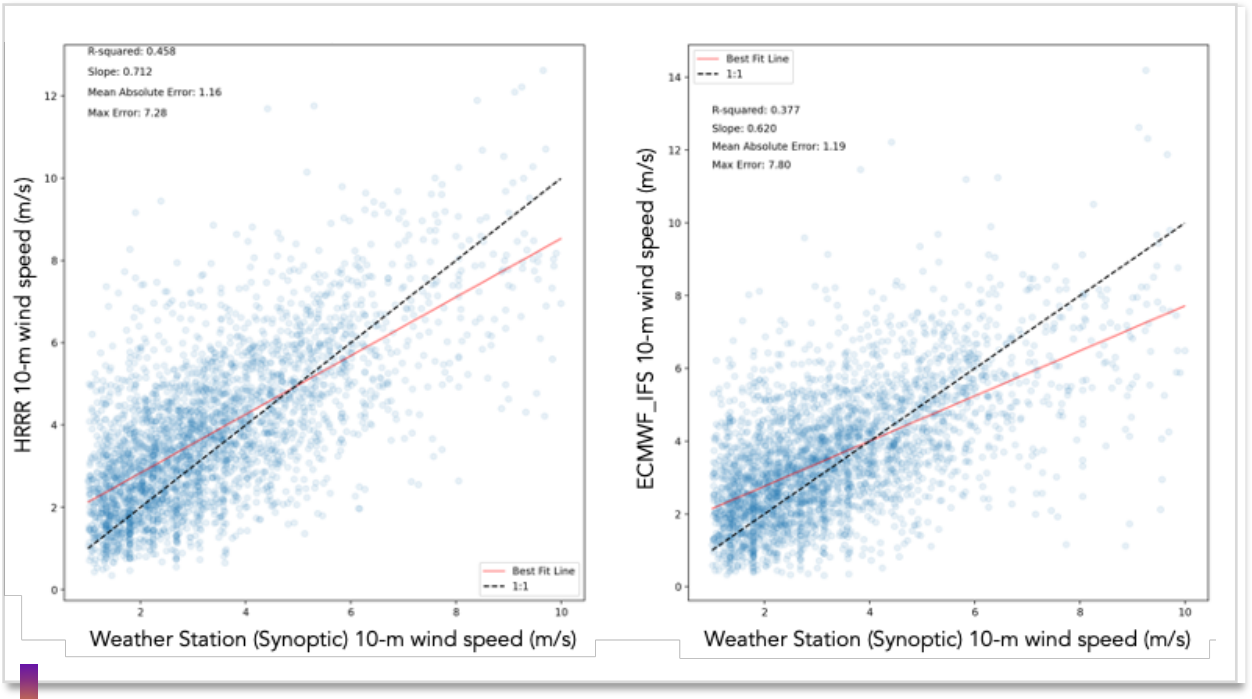

Figure 11. Comparison of U10 wind speeds from the HRRR and ECMWF_IFS global data products to 10-m weather data pulled from the Synoptic Weather Data API (synopticdata.com).

In Equation 9, *L* is estimated as the max distance from the origin point of the plume to another point along the segmented plume's convex hull. For plumes covering large spatial distances, we impose a distance constraint such that the segmented plume mask is clipped to not exceed a 285 m radial extent from the origin of the plume. Therefore, $L = min\{max(hulldist), 285\ m\}$. The IME (Equation 8) is also only calculated within this clipped plume mask. This clipping procedure is employed to reduce bias that may enter into IME quantification due to differing surface and meteorological conditions across large plumes, intermittency of the emission rate of the source, and to limit potential merging of multiple plumes downwind of their sources.

3.0 Data Handling, Storage and Delivery

3.1 Data Availability and Data Portal

A list of Carbon Mapper's SEP-relevant data products is shown in Table 2. Plume quantifications and attribution (L3B) products for the EPA's Super Emitter Program (SEP) are generated by Carbon Mapper's internal data platform within 72 hours of collection and will be provided to EPA via the SEP portal. L1B radiance data is permanently archived and is available to EPA upon request.

Carbon Mapper's quantified methane plumes and imagery are published in a variety of georeferenced file formats on our data portal: https://data.carbonmapper.org. For a complete list of data products, please refer to Carbon Mapper's Data Product Guide. Most processed products are published to our portal in most cases with a minimum latency of 30 days after collection. Data on the Carbon Mapper Portal is available for public, non-commercial use and may not be redistributed or republished without permission. For other use cases and custom licenses, please contact Carbon Mapper.

Description	File Type	Format	Latency
L3B Fully processed plume images with operator attribution, plume origin latitude and longitude, detection date and time	Tabular and associated raster data	CSV, GeoTIFF, PNG, GeoJSON	15 days
L4A Quantified plume emission rate with uncertainty	Tabular and associated raster data	CSV, GeoTIFF, PNG, GeoJSON	15 days

Table 2. Summary of Carbon Mapper Data products relevant to this application. An up-to-date copy of Carbon Mapper's full data products guide is available at https://carbonmapper.org/resources/technical-resources

3.2 Archiving of radiance data

After delivery to Carbon Mapper, calibrated radiance data is duplicated and permanently archived. Radiance data is not published, but archived raw radiance data from aircraft campaigns can be provided to select research partners upon request, or is available on the ORNL DAAC and delivered directly by JPL. Carbon Mapper permanently archives calibrated radiance data so that it can be reprocessed using the most up to date algorithms, as needed.

3.2 Methane Quick Look Data

For airborne campaigns, Carbon Mapper may choose to provide "quick look" methane data within 72 hours to collaborating partners. This data is processed in the same way as final data, but uses preliminary meteorological data to provide emissions estimates for plumes. Preliminary data has a variety of uses that can unlock rapid mitigation and provide feedback to partners. All preliminary data is subject to revision based on Carbon Mapper's QA/QC process. Once final Carbon Mapper obtains final wind products and finishes internal QA/QC review, airborne data is published on the Carbon Mapper data portal as quickly as described in Table 2.

4.0 Validation of Performance

Traditional approaches for calibration of column average gas mixing ratios (e.g., using a ground network like the Total Carbon Column Observing Network (TCCON)) are not readily applicable for application of validating plume enhancements. Generally, validation of methane data products occurs at L4 through controlled release experiments or comparison with independent evaluation of emissions (e.g., simultaneous mass-balance observations).

Carbon Mapper has considerable experience applying its CMF algorithms in blinded controlled releases for AVIRIS-class airborne instruments.These studies have shown that airborne platforms reliably detect emissions well below 100 kg/h (minimum detection limits for 3 m/s winds ranging from 10 to 45 kg/h) and show low bias against metered emission rates (Figure 12; El Abbadi et al., 2024).

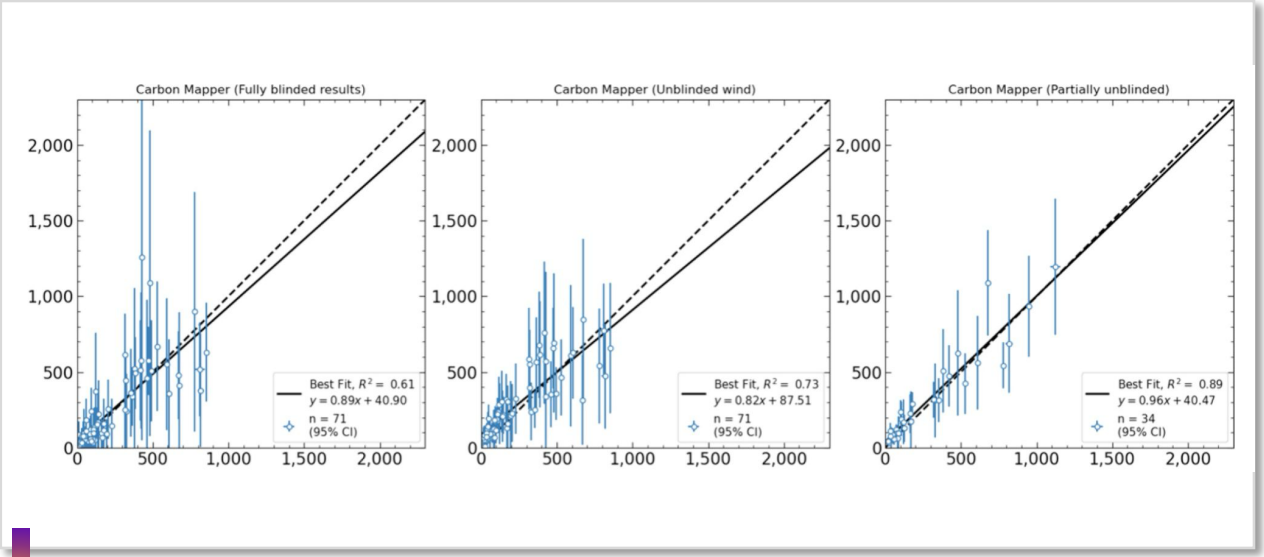

Figure 12. Summary of Carbon Mapper's airborne controlled release studies as reported in El Abbadi et al., 2024.

Carbon Mapper uses blinded and unblinded controlled release testing (El Abbadi, et al., 2024) to constrain and validate its emission rate calculation methodology. In addition, simultaneous observations with independent measurement methods such as in-situ mass balance flights (Cusworth et at., 2024), and years of application in field surveys including feedback from regulators and operators following site-level inspections are used where available.

Carbon Mapper continues to refine algorithms as more controlled release experiments are performed. Any modifications to Carbon Mapper algorithms from L2-L4 are only undertaken when they significantly improve correlation and bias against controlled validation datasets and other independent benchmarks (e.g., cross-comparison with other instrument platforms).

4.1 Detection Thresholds

Carbon Mapper reports both minimum detection limit (MDL) and 90% probability of detection (90% POD) for methane emission rates. For individual plumes, both metrics are highly dependent on surface reflectance (albedo), solar zenith angle at time of collection, flight altitude and meteorological conditions (especially wind speed). From blinded controlled release experiments performed in 2021-2022 (El Abbadi et al., 2024; Ayasse et al., 2023), Carbon Mapper detected plumes lower than 10 kg/h, and estimate a 90% POD of 45 kg/h for 3 m/s wind speed.

4.2 Uncertainty Characterization

All published plumes include both a mass emission rate estimate and a quantification uncertainty. Carbon Mapper reports a 1-sigma standard deviation uncertainty. In most cases, the dominant source of uncertainty is in wind speed.

Uncertainties in emission estimates are calculated by summing in quadrature elements that contribute to variability in emissions:

$$\sigma_q = \sqrt{\left(\frac{\partial Q}{\partial U}\sigma_U\right)^2 + \left(\frac{\partial Q}{\partial IME}\sigma_{IME}\right)^2 + \left(\frac{\partial Q}{\partial L}\sigma_L\right)^2} \quad (10)$$

Where

$$\sigma_{IME} = \frac{\partial Q}{\partial IME}\sigma_N + \frac{\partial Q}{\partial \Omega}\sigma_\Omega \quad (11)$$

In Equation 10 the $\left(\frac{\partial Q}{\partial U}\sigma_U\right)$term represents the uncertainty due to wind speed, which we estimate by computing the standard deviation of 10-m wind estimates across the hour before and after the plume detection. The $(\frac{\partial Q}{\partial IME}\sigma_{IME})$ term is decomposed into two components, first uncertainty due to masking, which we parameterize as the standard deviation of IME estimates across all segmented plume masks calculated for optimal candidate crop/percentile masks, and second uncertainty due to the retrieval, which was estimate as the standard deviation of concentration enhancements outside of the segmented plume mask. Finally, the $(\frac{\partial Q}{\partial L}\sigma_L)$ represents an irreducible uncertainty term due to the pixel resolution of the instrument and how it affects the estimate of plume length *L*.

4.3 Limitations

The process Carbon Mapper uses to quantify methane emissions from imaging spectrometer data (calibrated radiance cubes) is broadly applicable and sensor agnostic for airborne deployments ranging from 10,000 to 42,000 ft (3-14 km) above ground level. Environmental conditions (e.g. cloudy conditions, low sun angles, very low or very high wind speeds) that are unsuitable for deployment are typically the only limiting factors for data collection. Collection artifacts (surface effects, low albedo, open gas flaring, etc.) can limit detection of methane plumes, are flagged and evaluated during the QA/QC process described in Carbon Mapper's QC guide. A complete table of method interferences and their remedies are provided in Table 2 of Carbon Mapper's formal ATM document.

5.0 References

Asner, G. P., et al., Carnegie Airborne Observatory-2: Increasing science data dimensionality via high-fidelity multi-sensor fusion. Remote Sensing of Environment 2012, 124, 454−465.

Ayasse, A., *et al.,,* 2023. Performance and Sensitivity of Column-Wise and Pixel-Wise Methane Retrievals for Imaging Spectrometers. *Atmospheric Measurement Techniques* 16 (24): 6065–74.

Carbon Mapper L2b: Methane and Carbon Dioxide Emission Quantification for Satellites Algorithm Theoretical Basis Document. Most up-to-date version available at https://carbonmapper.org.

Carbon Mapper L3/L4: Methane and Carbon Dioxide Emission Quantification for Satellites Algorithm Theoretical Basis Document. Most up-to-date version available at https://carbonmapper.org/resources/technical-resources

Carbon Mapper Product Guide: Data Definition & Specification document. Most up-to-date version available at https://carbonmapper.org/resources/technical-resources

Carbon Mapper Quality Control Guide. Most up-to-date version available at https://carbonmapper.org/resources/technical-resources

Chapman, J.W. *et al.*, Spectral and Radiometric Calibration of the Next Generation Airborne Visible Infrared Spectrometer (AVIRIS-NG), *Remote Sens.* **2019**, *11*(18), 2129; https://doi.org/10.3390/rs11182129

Cusworth, D.H., *et al.*, 2021. Intermittency of Large Methane Emitters in the Permian Basin. *Environmental Science & Technology Letters* 8 (7): 567–73.

Cusworth, D.H., *et al.,* 2022, Strong Methane Point Sources Contribute a Disproportionate Fraction of Total Emissions Across Multiple Basins in the United States. *Proceedings of the National Academy of Sciences* 119 (38).

Cusworth, D.H., *et al.,* 2024, Quantifying methane emissions from United States landfills. Science 383 (6690): 1499-1504. https://doi.org/10.1126/science.adi7735

Duren, R. M. *et al.,* California's methane super-emitters. Nature 2019, 575, 180−184.

El Abbadi, S. H., *et al.,* Technological Maturity of Aircraft-Based Methane Sensing for Greenhouse Gas Mitigation, *Environ. Sci. Technol. 2024, 58, 9591−9600.*

Foote, M.D., Dennison, P.E., Sullivan, P.R., O'Neill, K.B., Thorpe, A.K., Thompson, D.R., Cusworth, D.H., Duren, R. and Joshi, S.C., 2021. Impact of scene-specific enhancement spectra on matched filter greenhouse gas retrievals from imaging spectroscopy. Remote Sensing of Environment, 264, p.112574.

Green, R.O. *et al*., "Airborne Visible/Infrared Imaging Spectrometer 3 (AVIRIS-3)," *2022 IEEE Aerospace Conference (AERO)*, Big Sky, MT, USA, 2022, pp. 1-10, doi: 10.1109/AERO53065.2022.9843565.

Hamlin, L., *et al.,* Imaging spectrometer science measurements for terrestrial ecology: AVIRIS and new developments. *Aerospace Conference,* IEEE (2011).

Mouroulis, P, R.O. Green, "Review of high fidelity imaging spectrometer design for remote sensing," Opt. Eng. 57(4), 040901 (2018), doi: 10.1117/1.OE.57.4.040901.

Sherwin, E.D., et al., 2024, US oil and gas system emissions from nearly one million aerial site measurements. *NATURE* 627, 328–334.

Thompson, D.R., *et al.,* Real-time remote detection and measurement for airborne imaging spectroscopy: a case study with methane. *Atmos. Meas. Tech., **8*** (10), 4383-4397 (2015).

Thorpe, A.K., *et al.*, 2021. Improved methane emission estimates using AVIRIS-NG and an Airborne Doppler Wind Lidar. *Remote Sensing of Environment*, *266*, p.112681.